Journal of Systems Engineering and Electronics
Vol. 37, No. 3, June 2026, pp.1019 – 1029

Fault-tolerant control of hypersonic morphing vehicle based on the predefined-time disturbance observer

LI Yiheng[1], ZHANG Wenjie[2,*], WANG Mingkai[3], XIA Qunli[1], and LIU Yangxin[1]

1. School of Aerospace Engineering, Beijing Institute of Technology, Beijing 100081, China;
2. Beijing Institute of Electronic System Engineering, Beijing 100854, China;
3. Hangzhou Innovation Institute, Beihang University, Hangzhou 311115, China

Abstract: To address the attitude control problem under the uncertainty, external disturbance, and actuator failure, a predefined-time fault-tolerant control method based on a predefined time disturbance observer is proposed. First, the dynamics model of hypersonic morphing vehicle (HMV) is established, and the control system is designed as an outer-loop attitude angle control loop and an inner-loop angular rate control loop considering the actuator failure problem. Secondly, a predefined-time disturbance observer is designed to estimate the comprehensive disturbances, and compensate in the control law. By integrating back-stepping control with predefined-time theory, a predefined-time attitude tracking control method is proposed, enabling the convergence time of the attitude tracking error to be designed through a simple parameter. Rigorous Lyapunov function analysis has demonstrated that the attitude tracking error can converge to an arbitrarily small neighborhood around the origin within a predefined time, and all signals in the closed-loop system are bounded. Finally, comparative simulations validate the effectiveness of the proposed method.

Keywords: hypersonic morphing vehicle (HMV), actuator failure, predefined-time disturbance observer, predefined-time fault-tolerant control.

DOI: 10.23919/JSEE.2026.000125

1. Introduction

Hypersonic morphing vehicles are capable of altering their aerodynamic configurations according to mission requirements to improve the performance [1]. However, with the change of the aerodynamic configurations of hypersonic morphing vehicle (HMV), its moment of inertia, mass distribution, aerodynamic force, and aerodynamic moment will also change significantly, which imposes strong nonlinearities, disturbances, and coupling on HMV [2,3]. Meanwhile, due to the complex structure and harsh flight conditions, HMV are more susceptible to actuator failures leading to performance degradation or even loss of control. Therefore, designing a high-reliability attitude controller with high tracking precision and fast convergence for HMV is of great significance.

The existing attitude control methods of HMV are roughly categorized into linear and nonlinear control methods [4]. Linear control methods encompass proportional-integral-differential (PID) [5], linear parameter varying (LPV) [6–8], gain scheduled control [9], etc. These methods are widely employed in early research due to their advantages of simple structure and ease in parameter tuning. Nevertheless, most linear control methods need to linearize the dynamic model around the equilibrium point and omit the nonlinear characteristics, which leads to the limitations of such methods in solving the attitude control problem of HMV with strong nonlinearity. The back-stepping control method is a commonly-used nonlinear control method for solving the attitude control problem of morphing aircraft [10–13]. To deal with the HMV attitude control problem, back-stepping control methods are usually combined with disturbance observers [14–17]. The disturbance observer can accurately estimate the disturbance and make compensations in the control law by reconstructing the external uncertain information, which is one of the most effective methods to suppress the uncertain disturbance and improve the robustness of the control system.

To ensure the rapid convergence of tracking errors for HMV during high-dynamic flight and morphing processes, the finite-time control theory [18–20] and fixed-time control [21–25] are proposed based on the asymptotically stable method, which can enhance the transient performance of the control system. However, the convergence time of the finite-time control depends on the initial states of the system, and the convergence time of fixed-time control methods is complicated to design,

Manuscript received December 12, 2024.
*Corresponding author.

making it impossible to predefine through a simple parameter. Therefore, in recent years, predefined-time control theory has received widespread attention. In [26], Lyapunov-like conditions were studied to ensure a class of dynamical systems exhibit predefined-time stability, and effective proofs of the predefined-time stability and its equivalent conditions were provided. In [27], a novel predefined-time sliding mode control method based on the predefined-time neural network disturbance observer was proposed for attitude control during the large-scale morphing flight of the morphing vehicle. The proposed control method can track the attitude to the desired values within the predefined time.

The harsh flight environment and complex structure of HMV can easily lead to actuator failures, thus reducing control performance and system stability. In order to solve this problem, a variety of studies on fault-tolerant control for aircraft have been proposed [28–33]. Liang et al. [28] designed a back-stepping fault-tolerant controller based on the fixed-time observer to deal with the problem of the attitude control of the morphing aircraft, which enables stable control of a closed-loop system in case of partial actuator failure. Li et al. [29] proposed a back-stepping fault-tolerant control method based on the fixed-time neural network observer to address the tracking control problem of morphing aircraft with model uncertainties, external disturbances, and actuator faults, and the designed controller was proved to be more adaptive and robust to various uncertainties and disturbances. However, regarding the control problem of morphing aircraft, the existing fault-tolerant control methods rarely manage to simultaneously address the rapid convergence of tracking errors and the robustness of control when facing complex disturbances from multiple sources, and they also falls short of accurately predefining the convergence time for the errors of controllers and observers.

Motivated by the preceding discussion, a fault-tolerant control method based on a predefined-time disturbance observer is proposed for the attitude control of HMV with uncertainty, external disturbances, and actuator failure. The main contributions of this paper are as follows.

(i) A predefined-time fault-tolerant control method is developed based on predefined-time disturbance observer. Compared with the control methods in [22] and [28], the tracking error of the proposed controller is guaranteed to converge to an arbitrarily small neighborhood of the origin within a predefined-time, and the convergence time is simple to design and is determined by a parameter.

(ii) The predefined-time control theory is introduced to design the disturbance observers for estimating the comprehensive disturbances of the HMV under model uncertainties, external disturbances, and actuator failures. Compared to the method in [15], this approach significantly enhances the accuracy of disturbance estimation and control robustness, while also ensuring that the observer error converges within the predefined-time.

The rest of this paper is organized as follows. Section 2 introduces the attitude dynamics model of HMV with actuator failure. Section 3 designs the predefined-time disturbance observer, and the predefined-time fault-tolerant controller, and proves the stability of the system. Section 4 demonstrates the superiority of the proposed control method by comparative simulation. Section 5 presents the conclusive remarks and discusses the future works.

2. Modeling and preliminaries

In this section, firstly, the attitude dynamics model of HMV is established and converted into control-oriented state space equations. Secondly, a fault-tolerant control model of HMV is established by considering the problem of actuator failure during the flight. Finally, the relevant lemmas and theorems used in the subsequent controller design and proof are given.

2.1 Attitude dynamics model of HMV

The configuration schematic of the HMV with a variable sweep angle investigated in this paper is shown in Fig. 1, where ζ represents the sweep angle.

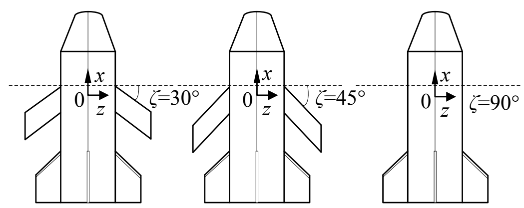

Fig. 1 Schematic diagram of the HMV configuration

Considering the attitude control problem during the reentry phase, the dynamics model of the HMV can be expressed as follows:

$$\begin{cases} \dot{\boldsymbol{x}}_1 = \boldsymbol{f}_1 + \boldsymbol{g}_1\boldsymbol{x}_2 + \boldsymbol{d}_1 \\ \dot{\boldsymbol{x}}_2 = \boldsymbol{f}_2 + \boldsymbol{g}_2\boldsymbol{u} + \boldsymbol{d}_2 \end{cases} \tag{1}$$

where $\boldsymbol{x}_1 = [\alpha, \beta, \gamma]^{\mathrm{T}}$ denotes the attitude angle vector consisting of angle of attack, sideslip angle and bank angle; $\boldsymbol{x}_2 = [\omega_{x1}, \omega_{y1}, \omega_{z1}]^{\mathrm{T}}$ denotes angular rate vector consisting of the angular rates of the roll, pitch, and yaw channels. $\boldsymbol{u} = [\delta_x, \delta_y, \delta_z]^{\mathrm{T}}$ denotes the system control input vector consisting of the roll elevator deflection, yaw elevator deflection, and pitch elevator deflection. $\boldsymbol{d}_1$, $\boldsymbol{d}_2$ denote comprehensive disturbances caused by factors such as model uncertainties and external disturbances.

The rest of the components $\boldsymbol{f}_1$, $\boldsymbol{g}_1$, $\boldsymbol{f}_2$, $\boldsymbol{g}_2$ in (1) can be expressed as $\boldsymbol{f}_1 = \begin{bmatrix} f_{11}, & f_{12}, & f_{13} \end{bmatrix}^{\mathrm{T}}$, f_{11}, f_{12}, f_{13} can be expressed as

$$\begin{cases} f_{11} = \dfrac{-Y + mg\cos\theta\cos\gamma}{mV\cos\beta} \\ f_{12} = \dfrac{N + mg\cos\theta\sin\gamma}{mV} \\ f_{13} = \dfrac{Y(\tan\theta\sin\gamma + \tan\beta) + N\tan\theta\cos\gamma}{mV} - \\ \quad \dfrac{g\cos\theta\cos\gamma\tan\beta}{V} \end{cases}, \tag{2}$$

$$\boldsymbol{f}_2 = \begin{bmatrix} \dfrac{(J_y^2 + J_{xy}^2 - J_yJ_z)}{J_xJ_y - J_{xy}^2}\omega_y\omega_z + \dfrac{(J_z - J_x - J_y)J_{xy}}{J_xJ_y - J_{xy}^2}\omega_x\omega_z \\ \dfrac{(J_xJ_z - J_x^2 - J_{xy}^2)}{J_xJ_y - J_{xy}^2}\omega_x\omega_z + \dfrac{(J_x + J_y - J_z)J_{xy}}{J_xJ_y - J_{xy}^2}\omega_y\omega_z \\ \dfrac{(J_x - J_y)\omega_x\omega_y + J_{xy}(\omega_x^2 - \omega_y^2)}{J_z} \end{bmatrix} + \begin{bmatrix} \dfrac{J_yC_{mx0}\bar{q}S_{\mathrm{ref}}L_{\mathrm{ref}} + J_{xy}C_{my0}\bar{q}S_{\mathrm{ref}}L_{\mathrm{ref}}}{J_xJ_y - J_{xy}^2} \\ \dfrac{J_{xy}C_{mx0}\bar{q}S_{\mathrm{ref}}L_{\mathrm{ref}} + J_xC_{my0}\bar{q}S_{\mathrm{ref}}L_{\mathrm{ref}}}{J_xJ_y - J_{xy}^2} \\ \dfrac{C_{mz0}\bar{q}S_{\mathrm{ref}}L_{\mathrm{ref}}}{J_z} \end{bmatrix}, \tag{3}$$

$$\boldsymbol{g}_1 = \begin{bmatrix} -\cos\alpha\tan\beta & \sin\alpha\tan\beta & 1 \\ \sin\alpha & \cos\alpha & 0 \\ \cos\alpha\sec\beta & -\sin\alpha\sec\beta & 0 \end{bmatrix}, \tag{4}$$

$$\boldsymbol{g}_2 = \bar{q}S_{\mathrm{ref}}L_{\mathrm{ref}}\boldsymbol{JC} \tag{5}$$

where $\boldsymbol{J}$, $\boldsymbol{C}$ can be expressed as

$$\boldsymbol{J} = \begin{bmatrix} \dfrac{1}{J_xJ_y - J_{xy}^2} & 0 & 0 \\ 0 & \dfrac{1}{J_xJ_y - J_{xy}^2} & 0 \\ 0 & 0 & \dfrac{1}{J_z} \end{bmatrix}, \tag{6}$$

$$\boldsymbol{C} = \begin{bmatrix} J_y & J_{xy} & 0 \\ J_{xy} & J_x & 0 \\ 0 & 0 & 1 \end{bmatrix} \begin{bmatrix} C_{mx}^{\delta_x} & C_{mx}^{\delta_y} & C_{mx}^{\delta_z} \\ C_{my}^{\delta_x} & C_{my}^{\delta_y} & C_{my}^{\delta_z} \\ C_{mz}^{\delta_x} & C_{mz}^{\delta_y} & C_{mz}^{\delta_z} \end{bmatrix}, \tag{7}$$

where m denotes the mass of HMV, V denotes the flight velocity, θ denotes the flight path angle, g denotes the gravitational acceleration. $Y = L + F_{sy_v}$, where $L = \bar{q}S_{\mathrm{ref}}C_L$ denotes the lift and F_{sy_v} denotes the component of the deformation additional force in the y-axis of the velocity coordinate system. $N = Z + F_{sz_v}$, where $Z = \bar{q}S_{\mathrm{ref}}C_Z$ denotes the lateral force and F_{sz_v} denotes the component of the deformation inertia force in the z-axis of the velocity coordinate system. $\bar{q} = 0.5\rho V^2$ denotes the dynamic pressure, ρ denotes the atmosphere density. S_{ref} denotes the reference area. J_x, J_y, J_z denote the roll, yaw and pitch moments of inertia. J_{xy} denotes the inertial product of HMV. M_x, M_y, M_z denote roll, yaw, and pitch aerodynamic moments respectively, which can be expressed as $M_x = C_{mx}\bar{q}S_{\mathrm{ref}}L_{\mathrm{ref}}$, $M_y = C_{my}\bar{q}S_{\mathrm{ref}}L_{\mathrm{ref}}$, $M_z = C_{mz}\bar{q}S_{\mathrm{ref}}L_{\mathrm{ref}}$, where L_{ref} denotes the reference length. $\boldsymbol{M}_s = [\ M_{sx}, \quad M_{sy}, \quad M_{sz}\ ]^{\mathrm{T}}$ denotes the component of the inertia moment due to deformation in each axis of the elastic body coordinate system. The inertia forces and moments generated during deformation can be expressed as

$$\begin{cases} \boldsymbol{F}_s = -\displaystyle\sum_{i=1}^{2} m_i \frac{\mathrm{d}^2\boldsymbol{s}_i}{\mathrm{d}t^2} \\ \boldsymbol{M}_s = -\displaystyle\sum_{i=1}^{2}\left(m_i\boldsymbol{s}_i \times \frac{\mathrm{d}\boldsymbol{V}}{\mathrm{d}t} + m_i\boldsymbol{s}_i \times \frac{\mathrm{d}^2\boldsymbol{s}_i}{\mathrm{d}t^2}\right) + \sum_{i=1}^{2}\boldsymbol{s}_i \times m_i\boldsymbol{g} \end{cases} \tag{8}$$

where $\boldsymbol{s}_i$ denotes the position vector from the aircraft's center of mass to the wing's center of mass. $m_i (i = 1,2)$ denotes the mass of the wings on both sides of the HMV. The velocity vector $\boldsymbol{V}$ will be decomposed in the body coordinate system. The change in the sweep angle of HMV not only causes the inertial forces and moments but also leads to the change in aerodynamic forces and moments due to the transformation of the aerodynamic configuration.

The aircraft model and aerodynamic parameters in this paper utilize the data from [34]. The coefficients of aerodynamic force and aerodynamic moment can be expressed as

$$C_i = C_{i0}(\mathrm{Ma},\alpha,\beta,\zeta) + C_i^{\delta_x}(\mathrm{Ma},\alpha,\beta,\zeta)\delta_x + \\ C_i^{\delta_y}(\mathrm{Ma},\alpha,\beta,\zeta)\delta_y + C_i^{\delta_z}(\mathrm{Ma},\alpha,\beta,\zeta)\delta_z \tag{9}$$

where i=L, Z, mx, my, mz. The aerodynamic coefficients and aerodynamic moment coefficients are fitted to formulas related to seven variables including Mach Ma, angle of attack α, sideslip angle β, roll elevator deflection δ_x, yaw elevator deflection δ_y, pitch elevator deflection δ_z and sweep angle ζ. For example, $i = mz$ for the pitch moment coefficient, $C_{mz0}(\mathrm{Ma},\alpha,\beta,\zeta)$ denotes the pitch moment coefficient at $\delta_x = \delta_y = \delta_z = 0$, $C_{mz}^{\delta_x}(\mathrm{Ma},\alpha,\beta,\zeta)$ denotes the partial derivative of the pitch moment coefficient with respect to δ_x, $C_{mz}^{\delta_y}(\mathrm{Ma},\alpha,\beta,\zeta)$ denotes the partial derivative of the pitch moment coefficient with respect to δ_y, $C_{mz}^{\delta_z}(\mathrm{Ma},\alpha,\beta,\zeta)$ denotes the partial derivative of the pitch moment coefficient with respect to δ_z.

The singularities of the matrices $\boldsymbol{g}_1$ and $\boldsymbol{g}_2$ in (1) are analyzed below. Taking the determinant of matrix $\boldsymbol{g}_1$, it can be obtained that when $\beta \neq 90°$, $\boldsymbol{g}_1$ is a non-singular matrix. In matrix $\boldsymbol{g}_2$, the absolute values of the elements $C_{mx}^{\delta_x}$, $C_{my}^{\delta_y}$, and $C_{mz}^{\delta_z}$ along the main diagonal are much larger than the absolute values of the other elements, hence matrix $\boldsymbol{g}_2$ can be approximated as a diagonal matrix. For HMV under normal flight conditions, $\boldsymbol{g}_2$ is a non-singular matrix.

2.2 Actuator failure modelling

In this paper, the actuator model of HMV with the gain and bias faults can be represented as follows:

$$\boldsymbol{u}_{\mathrm{F}}(t)=\boldsymbol{\eta}(t)\boldsymbol{u}(t)+\boldsymbol{\Lambda}(t),\ \ t\geqslant t_{\mathrm{f}} \tag{10}$$

where $\boldsymbol{u}_{\mathrm{F}}(t)$ is the control input under actuator failure, $\boldsymbol{u}(t)$ is the control inputs to be designed, t_{f} is the occurrence time of the actuator faults, $\boldsymbol{\eta}(t)=\mathrm{diag}(\eta_1(t),\eta_2(t),\eta_3(t))$ is the contribution efficiency of the actuator satisfying $0\leqslant\eta_i(t)\leqslant 1\ \ (i=1,2,3)$. $\boldsymbol{\Lambda}(t)=[\Lambda_1(t),\Lambda_2(t),\Lambda_3(t)]^{\mathrm{T}}$ is the actuator fault biases satisfying $|\Lambda_i(t)|\leqslant\bar{\Lambda}(t)$ $(i=1,2,3)$, $\bar{\Lambda}(t)$ is a positive constant. Therefore, the fault-tolerant model of HMV considering actuator failures is represented as follows:

$$\begin{cases}\dot{\boldsymbol{x}}_1=\boldsymbol{f}_1+\boldsymbol{g}_1\boldsymbol{x}_2+\boldsymbol{d}_1\\ \dot{\boldsymbol{x}}_2=\boldsymbol{f}_2+\boldsymbol{g}_2\boldsymbol{u}+\boldsymbol{D}_2\end{cases} \tag{11}$$

where $\boldsymbol{D}_2=\boldsymbol{g}_2(\boldsymbol{\eta}-\boldsymbol{I})\boldsymbol{u}+\boldsymbol{g}_2\boldsymbol{\Lambda}+\boldsymbol{d}_2$.

Remark 1 The actuator fault models employed for the exemplary HMV are also commonly seen in, for instance, [28–32]. This paper treats the effects of actuator faults on aircraft, model uncertainty, and disturbances generated by morphing process as comprehensive disturbances, which is observed based on predefined-time disturbance observer and compensated in control law.

Remark 2 Predefined-time, in essence, is a pre-designed convergence time that utilizes the predefined-time stability theory to achieve the pre-design of the convergence time of tracking error. In this paper, this theory is applied to the HMV control system, enabling the tracking error and the disturbance estimation error to converge to an arbitrarily small neighborhood within the predefined-time. As an important extension of the finite-time stability theory and the fixed-time stability theory, the predefined-time stability theory not only effectively overcomes the problem of initial dependence in traditional finite-time control, but also breaks through the limitation of the implicit correlation between the convergence time and parameters in fixed-time control.

3. Controller design

In this section, a predefined-time fault-tolerant controller based on predefined-time disturbance observer is designed for HMV to achieve accurate tracking of attitude angle commands. The controller scheme is illustrated in Fig. 2, where the control system is decomposed into an outer-loop attitude angle tracking control system and an inner-loop attitude angular rate tracking control system. It can be seen from Fig 2 that the output of the outer-loop attitude angle tracking control system is processed through a first-order command filter, which subsequently serves as the input for the inner-loop angular velocity tracking control system. The inner-loop system generates the final control law, establishing a closed-loop control system through the HMV dynamic system.

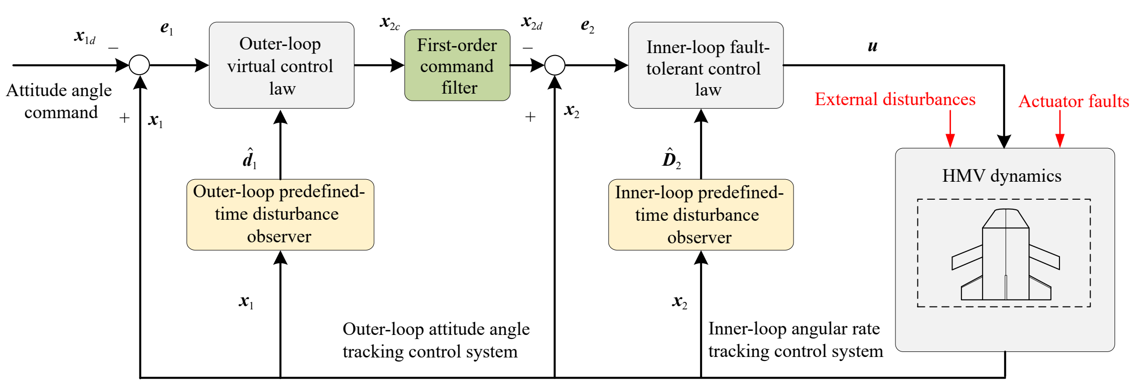

Fig. 2 Controllor scheme

The design approach of the controller is as follows. Firstly, a predefined-time disturbance observer is designed based on the predefined-time convergence control theory, and the convergence proof of the observer error is given. Then, a predefined-time fault-tolerant controller is designed based on the predefined-time theory, and a predefined-time disturbance observer is used to observe the comprehensive disturbances generated by the model uncertainty, the external disturbances and actuator failures, and to compensate them in the control law. Finally, the stability of the control system is proved based on Lyapunov stability theory and predefined-time control theory.

3.1 Design of predefined-time disturbance observer

According to (11), the general form of the dynamical model of HMV can be expressed as $\dot{\boldsymbol{x}} = \boldsymbol{f} + \boldsymbol{g}\boldsymbol{u} + \boldsymbol{d}$, where $\boldsymbol{u}$ is the control input, $\boldsymbol{f}$ and $\boldsymbol{g}$ are the known terms in the dynamics model, and $\boldsymbol{d}$ is the disturbance to be observed. The predefined-time disturbance observer is designed as

$$\begin{cases} \dot{\hat{\boldsymbol{x}}} = \boldsymbol{f} + \boldsymbol{g}\boldsymbol{u} + \hat{\boldsymbol{d}} + \dfrac{(2^{-p}\boldsymbol{e}^3 + 2^{1-2p}\lambda^{2-p}\boldsymbol{e}^{2p-1})}{(1-p)T_c\lambda} \\ \dot{\hat{\boldsymbol{d}}} = \dfrac{a}{(1-p)T_c\lambda}(2^{-p}\boldsymbol{e}^3 + 2^{1-2p}\lambda^{2-p}\boldsymbol{e}^{2p-1}) \end{cases} \tag{12}$$

where $\hat{\boldsymbol{x}}$ is an estimate of the system state $\boldsymbol{x}$, $\hat{\boldsymbol{d}}$ is an estimate of the disturbance $\boldsymbol{d}$. $a > 0$ is the gain of the predefined-time disturbance observer. $\boldsymbol{e} = \boldsymbol{x} - \hat{\boldsymbol{x}}$ is the estimation error of the system state, and the time derivative of $\boldsymbol{e}$ is

$$\dot{\boldsymbol{e}} = \dot{\boldsymbol{x}} - \dot{\hat{\boldsymbol{x}}} = \boldsymbol{d} - \hat{\boldsymbol{d}} - \frac{(2^{-p}\boldsymbol{e}^3 + 2^{1-2p}\lambda^{2-p}\boldsymbol{e}^{2p-1})}{(1-p)T_c\lambda}. \tag{13}$$

The stability of the predefined-time disturbance observer and the convergence of the disturbance observer errors will be proved subsequently.

3.2 Design of predefined-time fault-tolerant controller

Based on the back-stepping control method, the control system is divided into the outer-loop attitude angle tracking control system and the inner-loop angular rate tracking control system. $\boldsymbol{x}_{1d} = [\ \alpha_d,\ \ \beta_d,\ \ \gamma_d\ ]^{\mathrm{T}}$ is the attitude angle command from the guidance system. The tracking error of the outer-loop attitude angle is $\boldsymbol{e}_1 = \boldsymbol{x}_1 - \boldsymbol{x}_{1d}$, the tracking error of the inner-loop angular rate is $\boldsymbol{e}_2 = \boldsymbol{x}_2 - \boldsymbol{x}_{2d}$, where $\boldsymbol{x}_{2d}$ is the output of the first-order filter associated with the outer-loop virtual control law. Design the first order filter of the virtual control law as

$$\tau_2\dot{\boldsymbol{x}}_{2d} + \boldsymbol{x}_{2d} = \boldsymbol{x}_{2c} \tag{14}$$

where τ_2 is the filter parameter. $\boldsymbol{x}_{2c}$ is the virtual control law, which will be designed subsequently. In this paper, we define $\boldsymbol{x}_{2d}(0) = \boldsymbol{x}_{2c}(0)$ and ignore the filter error. The design of the predefined-time fault-tolerant controller is described below.

Step 1 For the outer-loop attitude angle control system, the time derivative of $\boldsymbol{e}_1$ is

$$\dot{\boldsymbol{e}}_1 = \boldsymbol{f}_1 + \boldsymbol{g}_1\boldsymbol{x}_2 + \boldsymbol{d}_1 - \dot{\boldsymbol{x}}_{1d}. \tag{15}$$

Design the virtual control law $\boldsymbol{x}_{2c}$ of the outer-loop attitude angle control system as

$$\boldsymbol{x}_{2c} = \boldsymbol{g}_1^{-1}(-\boldsymbol{f}_1 - \hat{\boldsymbol{d}}_1 + \dot{\boldsymbol{x}}_{1d} - \\ \frac{1}{(1-p)T_c\lambda}(2^{-p}{\boldsymbol{e}_1}^3 + 2^{1-2p}\lambda^{2-p}{\boldsymbol{e}_1}^{2p-1})) \tag{16}$$

where $\lambda > 0,\ 0 < p < 1$. $\hat{\boldsymbol{d}}_1$ is an estimate of the comprehensive disturbance of the outer loop. According to (12), the predefined-time disturbance observer for the outer-loop attitude angle tracking control is designed as

$$\begin{cases} \dot{\hat{\boldsymbol{x}}}_1 = \boldsymbol{f}_1 + \boldsymbol{g}_1\boldsymbol{x}_2 + \hat{\boldsymbol{d}}_1 + \dfrac{(2^{-p}{\boldsymbol{e}_{10}}^3 + 2^{1-2p}\lambda^{2-p}{\boldsymbol{e}_{10}}^{2p-1})}{(1-p)T_c\lambda} \\ \dot{\hat{\boldsymbol{d}}}_1 = \dfrac{a_1}{(1-p)T_c\lambda}(2^{-p}{\boldsymbol{e}_{10}}^3 + 2^{1-2p}\lambda^{2-p}{\boldsymbol{e}_{10}}^{2p-1}) \end{cases} \tag{17}$$

where a_1 is the gain of the predefined-time disturbance observer, $\boldsymbol{e}_{10} = \boldsymbol{x}_1 - \hat{\boldsymbol{x}}_1$ is the state observer error. Substituting (16) into (15) yields

$$\dot{\boldsymbol{e}}_1 = -\frac{(2^{-p}{\boldsymbol{e}_1}^3 + 2^{1-2p}\lambda^{2-p}{\boldsymbol{e}_1}^{2p-1})}{(1-p)T_c\lambda} + \tilde{\boldsymbol{d}}_1 + \boldsymbol{g}_1\boldsymbol{e}_2 \tag{18}$$

where $\tilde{\boldsymbol{d}}_1 = \boldsymbol{d}_1 - \hat{\boldsymbol{d}}_1$ is the disturbance estimation error.

Step 2 For the inner-loop angular rate control system, the time derivative of $\boldsymbol{e}_2$ is

$$\dot{\boldsymbol{e}}_2 = \boldsymbol{f}_2 + \boldsymbol{g}_2\boldsymbol{u} + \boldsymbol{D}_2 - \dot{\boldsymbol{x}}_{2d}. \tag{19}$$

The control law $\boldsymbol{u}$ can be constructed as follows:

$$\boldsymbol{u} = \boldsymbol{g}_2^{-1}\left(-\frac{(2^{-p}{\boldsymbol{e}_2}^3 + 2^{1-2p}\lambda^{2-p}{\boldsymbol{e}_2}^{2p-1})}{(1-p)T_c\lambda} - \boldsymbol{f}_2 - \hat{\boldsymbol{D}}_2 + \dot{\boldsymbol{x}}_{2d} - \boldsymbol{g}_1^{\mathrm{T}}\boldsymbol{e}_1\right) \tag{20}$$

where $\lambda > 0,\ 0 < p < 1$. $\hat{\boldsymbol{D}}_2$ is an estimate of the comprehensive disturbance of the inner-loop angular rate control system. According to (12), the predefined-time disturbance observer for the inner-loop attitude angle tracking control is designed as

$$\begin{cases} \dot{\hat{\boldsymbol{x}}}_2 = \boldsymbol{f}_2 + \boldsymbol{g}_2\boldsymbol{u} + \hat{\boldsymbol{D}}_2 + \dfrac{(2^{-p}{\boldsymbol{e}_{20}}^3 + 2^{1-2p}\lambda^{2-p}{\boldsymbol{e}_{20}}^{2p-1})}{(1-p)T_c\lambda} \\ \dot{\hat{\boldsymbol{D}}}_2 = \dfrac{a_2}{(1-p)T_c\lambda}(2^{-p}{\boldsymbol{e}_{20}}^3 + 2^{1-2p}\lambda^{2-p}{\boldsymbol{e}_{20}}^{2p-1}) \end{cases} \tag{21}$$

where a_2 is the gain of the predefined-time disturbance observer, $\boldsymbol{e}_{20} = \boldsymbol{x}_2 - \hat{\boldsymbol{x}}_2$ is the state observer error. Substituting (20) into (19) yields

$$\dot{\boldsymbol{e}}_2 = -\frac{(2^{-p}{\boldsymbol{e}_2}^3 + 2^{1-2p}\lambda^{2-p}{\boldsymbol{e}_2}^{2p-1})}{(1-p)T_c\lambda} + \tilde{\boldsymbol{D}}_2 - \boldsymbol{g}_1^{\mathrm{T}}\boldsymbol{e}_1 \tag{22}$$

where $\tilde{\boldsymbol{D}}_2 = \boldsymbol{D}_2 - \hat{\boldsymbol{D}}_2$ is the disturbance estimation error.

3.3 Stability analysis

In this subsection, we first prove the convergence of the state observation errors and disturbance estimation errors of the predefined-time disturbance observer in Theorem 1. Subsequently, in Theorem 2, we establish the stability and convergence of the proposed control method, which relies on the results of Theorem 1.

Theorem 1 If the control system of the HMV employs predefined-time disturbance observers, the predefined-time disturbance observer can guarantee the closed loop system bounded, then the state observer errors $\boldsymbol{e}_{10}$, $\boldsymbol{e}_{20}$ and the disturbance estimation error $\tilde{\boldsymbol{d}}_1$, $\tilde{\boldsymbol{D}}_2$ can converge to the vicinity of zero within the predefined time.

Proof Consider the following Lyapunov function candidate:

$$V = \frac{1}{2}\boldsymbol{e}_{10}^{\mathrm{T}}\boldsymbol{e}_{10} + \frac{1}{2}\boldsymbol{e}_{20}^{\mathrm{T}}\boldsymbol{e}_{20}. \tag{23}$$

Take the first-order derivative of V.

$$\dot{V} = \boldsymbol{e}_{10}^{\mathrm{T}}\dot{\boldsymbol{e}}_{10} + \boldsymbol{e}_{20}^{\mathrm{T}}\dot{\boldsymbol{e}}_{20} \tag{24}$$

By combining (15) and (17), $\dot{\boldsymbol{e}}_{10}$ can be expressed as

$$\dot{\boldsymbol{e}}_{10} = \dot{\boldsymbol{x}}_1 - \dot{\hat{\boldsymbol{x}}}_1 = \tilde{\boldsymbol{d}}_1 - \frac{(2^{-p}{\boldsymbol{e}_{10}}^3 + 2^{1-2p}\lambda^{2-p}{\boldsymbol{e}_{10}}^{2p-1})}{(1-p)T_c\lambda}. \tag{25}$$

By combining (19) and (21), $\dot{\boldsymbol{e}}_{20}$ can be expressed as

$$\dot{\boldsymbol{e}}_{20} = \dot{\boldsymbol{x}}_2 - \dot{\hat{\boldsymbol{x}}}_2 = \tilde{\boldsymbol{D}}_2 - \frac{(2^{-p}{\boldsymbol{e}_{20}}^3 + 2^{1-2p}\lambda^{2-p}{\boldsymbol{e}_{20}}^{2p-1})}{(1-p)T_c\lambda}. \tag{26}$$

Substituting (25) and (26) into (24) yields

$$\begin{aligned}\dot{V} = \boldsymbol{e}_{10}^{\mathrm{T}}\tilde{\boldsymbol{d}}_1 - \frac{2^{2-p}\left(\frac{\boldsymbol{e}_{10}^{\mathrm{T}}\boldsymbol{e}_{10}}{2}\right)^2 + 2^{1-p}\lambda^{2-p}\left(\frac{\boldsymbol{e}_{10}^{\mathrm{T}}\boldsymbol{e}_{10}}{2}\right)^p}{(1-p)T_c\lambda} + \\ \boldsymbol{e}_{20}^{\mathrm{T}}\tilde{\boldsymbol{D}}_2 - \frac{2^{2-p}\left(\frac{\boldsymbol{e}_{20}^{\mathrm{T}}\boldsymbol{e}_{20}}{2}\right)^2 + 2^{1-p}\lambda^{2-p}\left(\frac{\boldsymbol{e}_{20}^{\mathrm{T}}\boldsymbol{e}_{20}}{2}\right)^p}{(1-p)T_c\lambda}.\end{aligned} \tag{27}$$

From Lemma 3 in [27], it can be derived that

$$\begin{aligned}\dot{V} \leqslant -\frac{2^{1-p}\left(\frac{\boldsymbol{e}_{10}^{\mathrm{T}}\boldsymbol{e}_{10}}{2} + \frac{\boldsymbol{e}_{20}^{\mathrm{T}}\boldsymbol{e}_{20}}{2}\right)^2}{(1-p)T_c\lambda} + \boldsymbol{e}_{10}^{\mathrm{T}}\tilde{\boldsymbol{d}}_1 - \\ \frac{2^{1-p}\lambda^{2-p}\left(\frac{\boldsymbol{e}_{10}^{\mathrm{T}}\boldsymbol{e}_{10}}{2} + \frac{\boldsymbol{e}_{20}^{\mathrm{T}}\boldsymbol{e}_{20}}{2}\right)^p}{(1-p)T_c\lambda} + \boldsymbol{e}_{20}^{\mathrm{T}}\tilde{\boldsymbol{D}}_2.\end{aligned} \tag{28}$$

According to Lemma 4 in [24] (Young's inequality), the following inequalities hold true:

$$\begin{cases}\boldsymbol{e}_{10}^{\mathrm{T}}\tilde{\boldsymbol{d}}_1 \leqslant \dfrac{\boldsymbol{e}_{10}^{\mathrm{T}}\boldsymbol{e}_{10}}{2} + \dfrac{\tilde{\boldsymbol{d}}_1^{\mathrm{T}}\tilde{\boldsymbol{d}}_1}{2} \\ \boldsymbol{e}_{20}^{\mathrm{T}}\tilde{\boldsymbol{D}}_2 \leqslant \dfrac{\boldsymbol{e}_{20}^{\mathrm{T}}\boldsymbol{e}_{20}}{2} + \dfrac{\tilde{\boldsymbol{D}}_2^{\mathrm{T}}\tilde{\boldsymbol{D}}_2}{2}\end{cases}, \tag{29}$$

$$\vartheta = \frac{\left(\boldsymbol{e}_{10}^{\mathrm{T}}\boldsymbol{e}_{10} + \tilde{\boldsymbol{d}}_1^{\mathrm{T}}\tilde{\boldsymbol{d}}_1 + \boldsymbol{e}_{20}^{\mathrm{T}}\boldsymbol{e}_{20} + \tilde{\boldsymbol{D}}_2^{\mathrm{T}}\tilde{\boldsymbol{D}}_2\right)}{2}. \tag{30}$$

According to Lemma 3 in [27] it follows that

$$\dot{V} \leqslant -\frac{(V^p(V+\lambda)^{2-p})}{(1-p)T_c\lambda} + \vartheta. \tag{31}$$

According to the Proposition 1 in [27], it can be proved that the state observer errors $\boldsymbol{e}_{10}$, $\boldsymbol{e}_{20}$ can converge to the vicinity of zero within the predefined time. Therefore $\boldsymbol{e}_{10}$, $\boldsymbol{e}_{20}$ have upper bounds. Then the following formula can be satisfied: $\lim\limits_{t\to\infty}\|\dot{\boldsymbol{e}}_{10}\| = 0$, $\lim\limits_{t\to\infty}\|\dot{\boldsymbol{e}}_{20}\| = 0$. According to the Proposition 1 in [27] and (13), when $t \geqslant T_c$, the disturbance estimation error $\dot{\boldsymbol{e}}_{10} = \tilde{\boldsymbol{d}}_1$, $\dot{\boldsymbol{e}}_{20} = \tilde{\boldsymbol{D}}_2$ stabilizes to zero asymptotically. □

Theorem 2 Considering the dynamics model of HMV in (11), with the predefined-time fault-tolerant controllers in (16) and (20), and the predefined-time disturbance observers in (17) and (21), all signals of the closed-loop control system can be stabilized and bounded, and the attitude tracking error $\boldsymbol{e}_1$ and $\boldsymbol{e}_2$ will also finally converge into the small regions within the predefined time.

Proof Consider the following Lyapunov function candidate:

$$V_1 = \frac{1}{2}\boldsymbol{e}_1^{\mathrm{T}}\boldsymbol{e}_1 + \frac{1}{2}\boldsymbol{e}_2^{\mathrm{T}}\boldsymbol{e}_2. \tag{32}$$

Take the first-order derivative of V_1.

$$\dot{V}_1 = \boldsymbol{e}_1^{\mathrm{T}}\dot{\boldsymbol{e}}_1 + \boldsymbol{e}_2^{\mathrm{T}}\dot{\boldsymbol{e}}_2 \tag{33}$$

Substituting (24) and (28) into (39) yields

$$\begin{aligned}\dot{V}_1 = -\frac{2^{2-p}\left(\left(\frac{\boldsymbol{e}_1^{\mathrm{T}}\boldsymbol{e}_1}{2}\right)^2 + \left(\frac{\boldsymbol{e}_2^{\mathrm{T}}\boldsymbol{e}_2}{2}\right)^2\right)}{(1-p)T_c\lambda} + \boldsymbol{e}_1^{\mathrm{T}}\tilde{\boldsymbol{d}}_1 - \\ \frac{2^{1-p}\lambda^{2-p}\left(\left(\frac{\boldsymbol{e}_1^{\mathrm{T}}\boldsymbol{e}_1}{2}\right)^p + \left(\frac{\boldsymbol{e}_2^{\mathrm{T}}\boldsymbol{e}_2}{2}\right)^p\right)}{(1-p)T_c\lambda} + \boldsymbol{e}_2^{\mathrm{T}}\tilde{\boldsymbol{D}}_2.\end{aligned} \tag{34}$$

According to Lemma 3 in [27], the following inequalities hold true:

$$\dot{V}_1 \leqslant -\frac{\left({V_1}^p(V_1+\lambda)^{2-p}\right)}{(1-p)T_c\lambda} + \vartheta_1 \tag{35}$$

where $\vartheta_1 = \boldsymbol{e}_1^{\mathrm{T}}\tilde{\boldsymbol{d}}_1 + \boldsymbol{e}_2^{\mathrm{T}}\tilde{\boldsymbol{D}}_2$. According to the Proposition 1 in [27] and Theorem 1, the attitude tracking error $\boldsymbol{e}_1$ and $\boldsymbol{e}_2$ will also finally converge into the small regions within the predefined time. Thereby the proof of Theorem 2 is completed. □

4. Simulation

In this section, the effectiveness of the predefined-time fault-tolerant control method for HMV based on the predefined-time disturbance observer is verified by comparative simulation. The simulation comprised two scenarios. Scenario 1 is the simulation of the attitude tracking control when the actuator is working normally and without external disturbances. Scenario 2 is the comparison simulation of attitude tracking control considering actuator faults and external disturbances. Scenario 2 is developed on the basis of Scenario 1, where the predefined-time T_c for the HMV is initially established. In both simulation scenarios, amplitude limits are imposed on the rudder deflection angle and its rate to ensure practical engineering applicability. Specifically, the rudder deflection angle is limited to $|\delta_z| \leqslant 30°$, $|\delta_y| \leqslant 20°$, $|\delta_x| \leqslant 20°$.

4.1 Scenario 1: nominal cases

In order to verify the effectiveness of the predefined-time fault-tolerant controller, several predefined-times are set in the simulation to analyze the effect of the predefined-times on the control effect. The predefined-times is set as $T_c = 2$ s, $T_c = 3$ s, $T_c = 5$ s, $T_c = 10$ s, $T_c = 15$ s, $T_c = 20$ s. Other parameters are assigned as $p = 0.9$, $\lambda = 0.5$ throughout simulations.

The initial values for the simulation of the attitude angle of the HMV are set to $[\alpha_0, \beta_0, \gamma_0]^{\mathrm{T}} = [15°, 2°, 0°]^{\mathrm{T}}$, and the initial values of the angular rate of the three channels are set to $0°/\mathrm{s}$. The altitude and velocity of the HMV are set to $h_0 = 30$ km, $V_0 = 2\,500$ m/s. The attitude angle command is set to $[\alpha_d, \beta_d, \gamma_d]^{\mathrm{T}} = [10°, 0°, 10°]^{\mathrm{T}}$. Simulation results of 0–20 s are shown in Fig. 3 and Fig. 4.

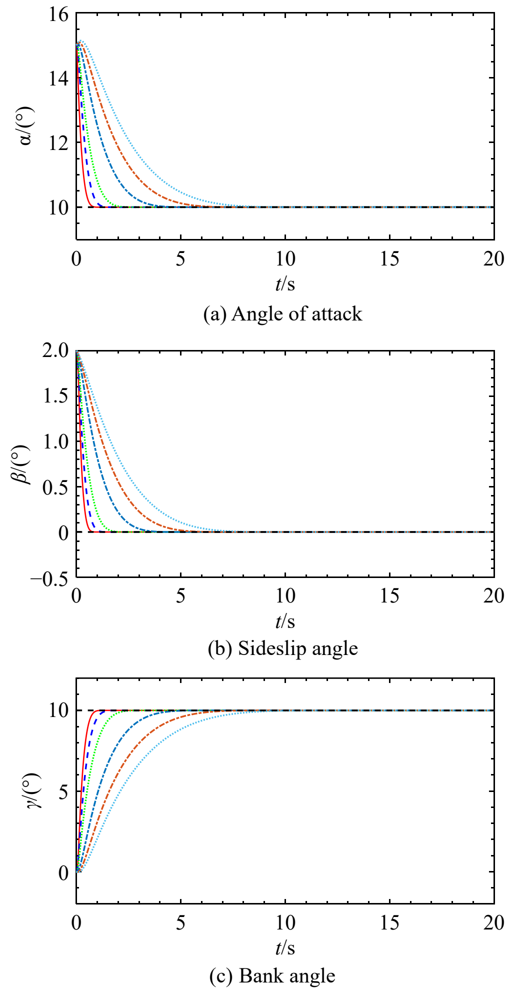

(a) Angle of attack

(b) Sideslip angle

(c) Bank angle

: T_c=2; : T_c=3; : T_c=5; : T_c=10; : T_c=15; : T_c=20; : γ_d.

Fig. 3 Attitude angle tracking curve

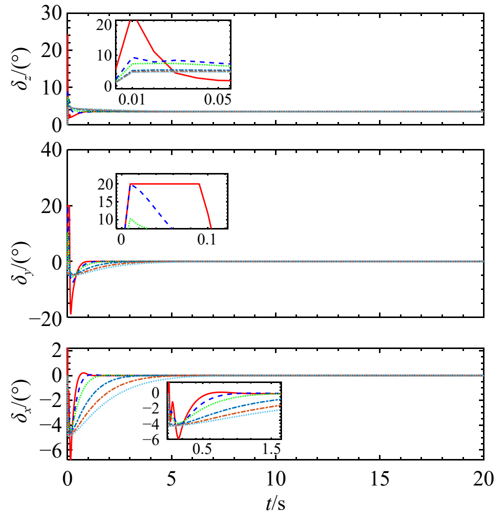

Fig. 4 Control input

The above simulation results indicate that the predefined-time fault-tolerant control methods can guarantee the attitude angle effectively tracks the commands under the different predefined-times, while the convergence time of the tracking error changes with the predefined-times.

The rate of convergence of the tracking error decreases as the predefined-time increases. From the partial enlarged view in Fig. 4, it can be seen that the rudder deflection curves of T_c=2 s and T_c=3 s reach the limit value at the initial moment. However, considering the actual engineering situation of the actuator, the rudder deflection angular rate should be within a reasonable range, and in this paper, the maximum value of the absolute value of the rudder deflection angular rate is limited to 300°/s. In order to balance the rapid convergence speed of tracking error with the reasonableness of the rudder deflection angular rate, $T_c = 5$ s is chosen for subsequent simulation.

4.2 Scenario 2: simulation cases with actuator faults

In this scenario, actuator failures, external disturbances, and the change of sweep angles are considered simultaneously. Two comparative methods are set up to compare with the method proposed in this paper, in which comparison method 1 uses the predefined-time disturbance observer designed in [15], marked as 'PTDO' in the simulation results, comparison method 2 uses the fixed time disturbance observer-based back-stepping fault-tolerant control method designed in [28], marked as 'FTDO' in the simulation results. The sweep angle of the aircraft changes from 30° to 90° between 15 s and 17 s, the curve of sweep angle is shown in Fig. 5. The parameters for the proposed controller are set as $p = 0.9$, $\lambda = 0.5$, $T_c = 5$, $a_1 = 50$, $a_2 = 50$, $\tau_2 = 0.01$. The uncertain external disturbances throughout the 50 s simulation are designed as follows:

$$\begin{cases} \boldsymbol{d}_1 = \left[0.05\sin\dfrac{\pi t}{30}, 0.05\sin\dfrac{\pi t}{30}, 0.05\sin\dfrac{\pi t}{30}\right]^{\mathrm{T}} \\ \boldsymbol{d}_2 = \left[2\sin\dfrac{\pi t}{5}, 12\sin\dfrac{\pi t}{5},\ \ 2\sin\dfrac{\pi t}{5}\right]^{\mathrm{T}} \end{cases}. \tag{36}$$

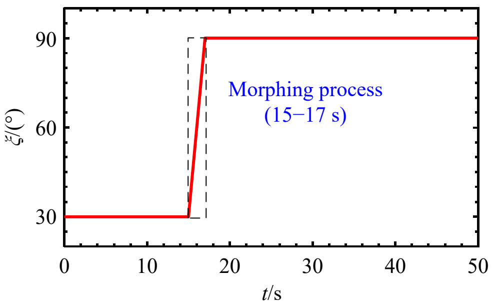

Fig. 5 Curve of sweep angle

Actuator failure at 25 s, the considered actuator failure are modeled as follows:

$$\boldsymbol{\eta} = \begin{cases} [1,1,1]^{\mathrm{T}},\ \ 0 \leqslant t < 25 \\ [0.8,0.8,0.7]^{\mathrm{T}},\ \ 25 \leqslant t \leqslant 50 \end{cases},$$

$$\boldsymbol{\Lambda} = \begin{cases} [0,0,0]^{\mathrm{T}},\ \ 0 \leqslant t < 25 \\ \begin{bmatrix} 0.02\sin\dfrac{\pi t}{2} \\ 0.03\sin\dfrac{\pi t}{2} \\ 0.02\sin\dfrac{\pi t}{2} \end{bmatrix},\ \ 25 \leqslant t \leqslant 50 \end{cases}. \tag{37}$$

The simulation results of Scenario 2 are shown in Fig. 6–Fig. 11. All three control methods can track the command accurately at 0–25 s, as shown in Fig. 6. However, when the actuator failure occurrs at 25 s, the tracking error of the comparison methods increases significantly, and the tracking error of angle of attack fails to converge after the actuator failure, as shown in Fig. 7. The attitude angle tracking errors of the proposed method are significantly smaller than those of the comparison method when the actuator failure is considered, and the convergence time of the tracking error is significantly smaller than that of the comparison method. The attitude angular rate curve and control input for the three channels are shown in Fig. 8 and Fig. 9, during the morphing process at $t = 15 - 17$ s, the pitch rudder deflection angle changes significantly. Outer-loop and inner-loop disturbance estimation values are shown in Fig. 10 and Fig. 11, it can be obtained that the inner loop disturbance observations are all markedly jittery when the actuator failure occurrs at 25 s.

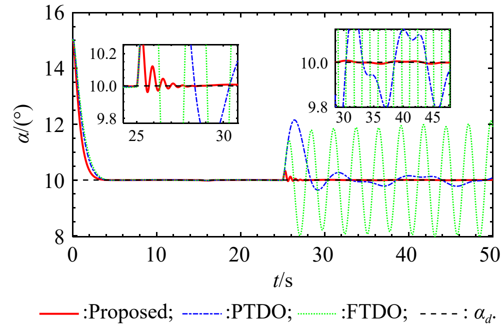

(a) Angle of attack

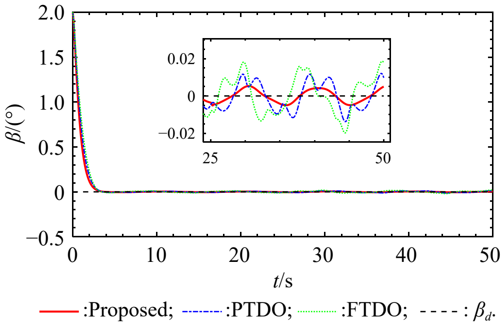

(b) Sideslip angle

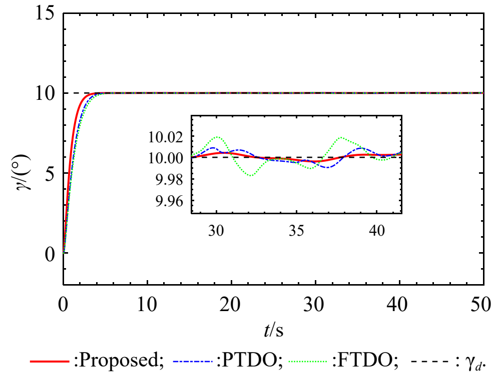

(c) Bank angle

Fig. 6 Attitude angle tracking response

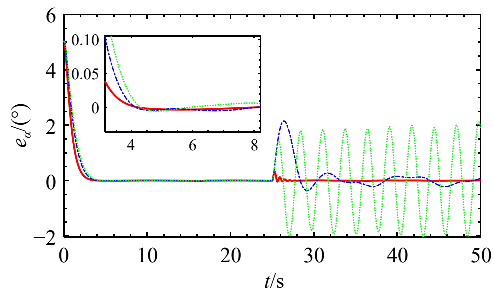

(a) Tracking error of angle of attack

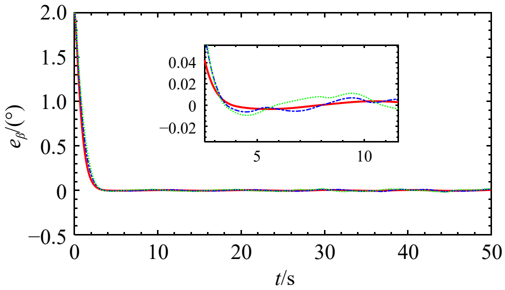

(b) Tracking error of sideslip angle

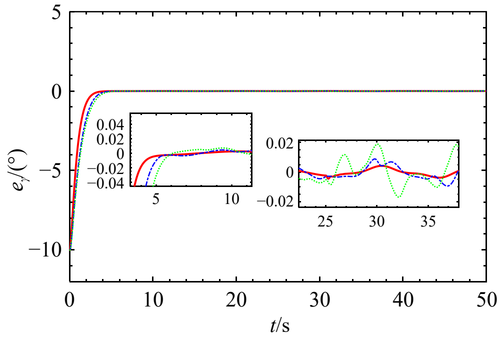

(c) Tracking error of bank angle

: Proposed; : PTDO; : FTDO.

Fig. 7 Tracking error of the attitude angle

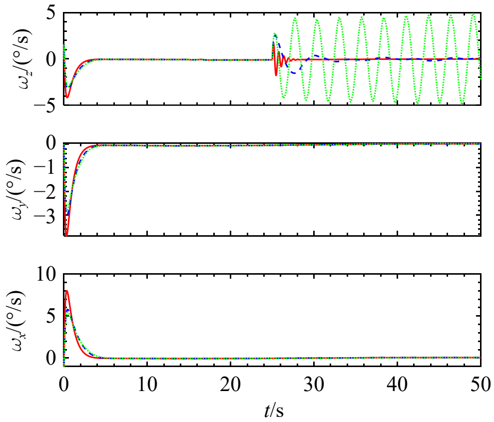

: Proposed; : PTDO; : FTDO.

Fig. 8 Attitude angular rate curve

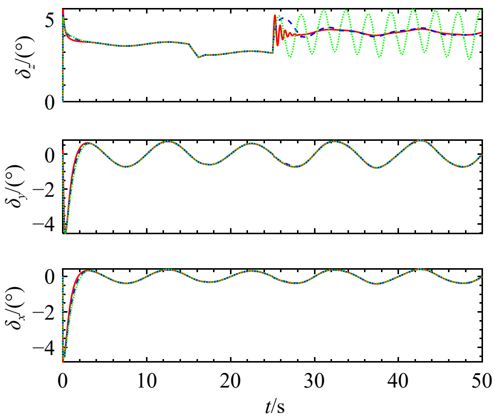

: Proposed; : PTDO; : FTDO.

Fig. 9 Control input

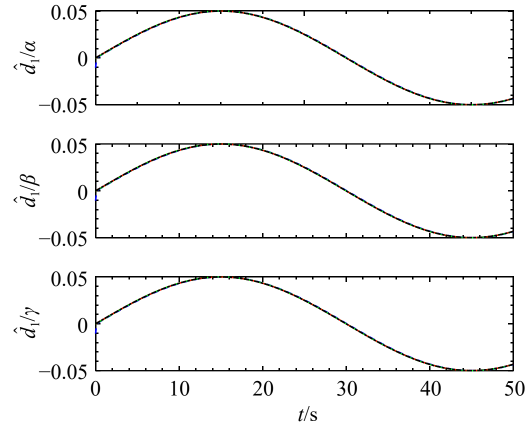

: Proposed; : PTDO; : FTDO; : d_1.

Fig. 10 Outer-loop disturbance estimation value

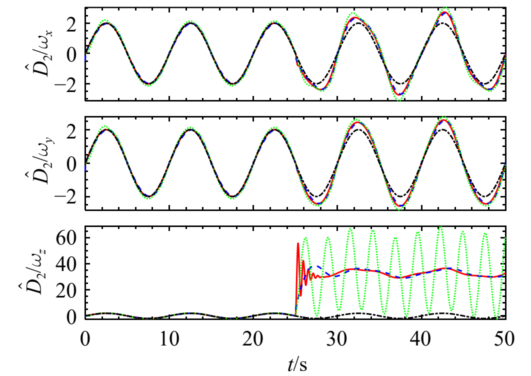

: Proposed; : PTDO; : FTDO; : d_2.

Fig. 11 Inner-loop disturbance estimation value

Comparison of the simulation results between Scenario 1 and Scenario 2 shows that for HMV with uncertainties, external disturbances, and time-varying actuator faults, the predefined-time fault-tolerant control method based on the predefined-time disturbance observer designed in this paper has higher tracking accuracy and faster transient response. The proposed control method can regulate the tracking error convergence time with T_c, which is superior regarding fast error convergence, robustness and stability.

5. Conclusions

This paper proposes a predefined-time fault-tolerant control method based on a predefined-time disturbance observer to address the attitude tracking control problem of HMV with model uncertainty, external disturbances and actuator failure. The advantages of the proposed method are demonstrated through numerical simulations. The novelties are as follows:

(i) A predefined-time fault-tolerant controller is proposed by integrating actual predefined-time convergence theory with backstepping control. This controller ensures that the attitude angle tracking error converges to an arbitrarily small neighborhood within a user-defined time, significantly improving the convergence speed of the control system. Moreover, the predefined-time parameter can be easily tuned through a single, straightforward parameter, greatly simplifying the control system design and reducing tuning complexity.

(ii) A predefined-time disturbance observer is developed based on predefined-time theory to accurately estimate composite disturbances arising from model uncertainties, external disturbances, and actuator faults. The observer guarantees that the estimation error converges within the predefined time, thereby enhancing the robustness and reliability of the control system in complex and uncertain environments.

In the future, research will be conducted on the jitter issues caused by the large gain of predefined-time disturbance observers, while also considering the errors of first-order filters in virtual control laws. In order to further improve the robustness of the control system under complex disturbances, adaptive neural networks or intelligent algorithms can also be introduced.

References

[1] BAO C Y, WANG P, TANG G J. Integrated method of guidance, control and morphing for hypersonic morphing vehicle in glide phase. Chinese Journal of Aeronautics, 2021, 34(5): 535–553.

[2] DONG C Y, LIU C, WANG Q, et al. Switched adaptive active disturbance rejection control of variable structure near space vehicles based on adaptive dynamic programming. Chinese Journal of Aeronautics, 2019, 32(7): 1684–1694.

[3] DAI P, FENG D Z, ZHAO J Q, et al. Asymmetric integral barrier Lyapunov function based dynamic surface control of a state-constrained morphing waverider with anti-saturation compensator. Aerospace Science and Technology, 2022, 131: 107975.

[4] CHU L, LI Q, GU F, et al. Design, modeling, and control of morphing aircraft: a review. Chinese Journal of Aeronautics, 2022, 35(5): 220–246.

[5] YAN B B, LI Y, DAI P, et al. Aerodynamic analysis, dynamic modeling, and control of a morphing aircraft. Journal of Aerospace Engineering, 2019, 32(5): 04019058.

[6] YUE T, WANG L X, AI J Q. Gain self-scheduled H_∞ control for morphing aircraft in the wing transition process based on an LPV model. Chinese Journal of Aeronautics, 2013, 26(4): 909–917.

[7] JIANG W L, WU K S, WANG Z L, et al. Gain-scheduled control for morphing aircraft via switching polytopic linear parameter-varying systems. Aerospace Science and Technology, 2020, 107: 106242.

[8] WU Q, LIU Z H, LIU F N, et al. LPV-based self-adaption integral sliding mode controller with L2 gain performance for a morphing aircraft. IEEE Access, 2019, 7: 81515–81531.

[9] JIANG W L, DONG C Y, WANG Q. A systematic method of smooth switching LPV controllers design for a morphing aircraft. Chinese Journal of Aeronautics, 2015, 28(6): 1640–1649.

[10] GONG L G, WANG Q, DONG C Y. Disturbance rejection control of morphing aircraft based on switched nonlinear systems. Nonlinear Dynamics, 2019, 96(2): 975–995.

[11] LI Y H, LIU D W, ZHOU H, et al. Adaptive backstepping control of morphing aircraft based on RBF neural networks. Proc. of the International Symposium on Aerospace Engineering and Systems 2023: 195−201.

[12] WU Z H, LU J C, ZHOU Q, et al. Modified adaptive neural dynamic surface control for morphing aircraft with input and output constraints. Nonlinear Dynamics, 2017, 87(4): 2367–2383.

[13] QIAO F X, SHI J P, QU X B, et al. Adaptive back-stepping neural control for an embedded and tiltable V-tail morphing aircraft. International Journal of Control, Automation and Systems, 2022, 20(2): 678–690.

[14] XIE S Z, CHEN Q. Predefined-time disturbance estimation and attitude control for rigid spacecraft. IEEE Trans. on Circuits and Systems II: Express Briefs, 2024, 71(4): 2089–2093.

[15] CHEN J Y, ZHANG H C, XIAO B, et al. Predefined-time observer-based nonsingular sliding-mode control for spacecraft attitude stabilization. IEEE Trans. on Circuits and Systems II: Express Briefs, 2024, 71(3): 1291–1295.

[16] ZHANG H C, HUANG H W, XIAO B, et al. Command-filtered incremental backstepping attitude control of spacecraft with predefined-time stability. Aerospace Science and Technology, 2024, 155(1): 109552.

[17] LI H, YANG H S, LIU Z C. Command filter-based adaptive predefined-time control for non-strict feedback nonlinear systems with unmodeled dynamics. Journal of the Franklin Institute, 2024, 361(12): 106936.

[18] SUN H B, LI S H, SUN C Y. Finite time integral sliding mode control of hypersonic vehicle. Nonlinear Dynamics, 2013, 73(1): 229–424.

[19] SUN J L, YI J Q, PU Z Q, et al. Adaptive fuzzy nonsmooth back-stepping output-feedback control for hypersonic vehicles with finite-time convergence. IEEE Trans. on Fuzzy Systems, 2020, 28(10): 2320–2034.

[20] TANG X N, ZHAI D, LI X J. Adaptive fault-tolerance control based finite-time backstepping for hypersonic flight vehicle with full state constrains. Information Sciences, 2020, 507: 53–66.

[21] POLYAKOV A. Nonlinear feedback design for fixed-time stabilization of linear control systems. IEEE Trans. on Automatic Control, 2012, 57(8): 2106–2110.

[22] WANG X, GUO J, TANG S J, et al. Fixed-time disturbance observer based fixed-time back-stepping control for an air-breathing hypersonic vehicl. ISA Transactions, 2019, 88: 233–245.

[23] DONG Z H, LI Y H, LV M L. Adaptive nonsingular fixed-time control for hypersonic flight vehicle considering angle of attack constraints. International Journal of Robust and Nonlinear Control, 2023, 33(12): 6754–6777.

[24] ZHANG Y C, MA M C, YANG X Y, et al. Disturbance-observer-based fixed-time control for 6-DOF spacecraft rendezvous and docking operations under full-state constraint. Acta Astronautica, 2023, 205: 225–238.

[25] SUN J L, YI J Q, PU Z Q, et al. Fixed-time sliding mode disturbance observer-based nonsmooth backstepping control for hypersonic vehicles. IEEE Trans. on Systems, Man, and Cybernetics: Systems, 2020, 50(11): 4377–4386.

[26] JIMÉNEZ-RODRÍGUEZ E, MUÑOZ-VÁZQUEZ A J, SÁNCHEZ-TORRES J D, et al. A Lyapunov-like characteri-

zation of predefined-time stability. IEEE Trans. on Automatical Control, 2020, 65(11): 4922–4927.

[27] LU X Y, WANG J Y, WANG Y H, et al. Neural network observer-based predefined-time attitude control for morphing hypersonic vehicles. Aerospace Science and Technology, 2024, 52: 109333.

[28] LIANG X H, WANG Q, XU B, et al. Back-stepping fault-tolerant control for morphing aircraft based on fixed-time observer. International Journal of Control, Automation and Systems, 2021, 19(12): 3924–36.

[29] LI Y H, WANG M K, XIA Q L. Back-stepping fault-tolerant control method of morphing aircraft based on fixed-time neural network observer. Journal of Aerospace Engineering, 2025, 38(2): 04024119.

[30] JU X Z, WEI C Z, XU H C, et al. Fractional-order sliding mode control with a predefined-time observer for VTVL reusable launch vehicles under actuator faults and saturation constraints. ISA Transactions, 2022, 129: 55–72.

[31] YUAN L H, WANG L D, XU J T. Adaptive fault-tolerant controller for morphing aircraft based on the L2 gain and a neural network. Aerospace Science and Technology, 2023, 132: 107985.

[32] XU S H, WEI C Z, ZHANG L T, et al. Neural network based adaptive nonsingular practical predefined-time fault-tolerant control for hypersonic morphing aircraft. Chinese Journal of Aeronautics, 2024, 37(4): 421–435.

[33] LIANG S, XU B, ZHANG Y M. Robust self-learning fault-tolerant control for hypersonic flight vehicle based on ADHDP. IEEE Trans. on Systems, Man, and Cybernetics: Systems, 2023, 53(9): 5295–5306.

[34] ZHANG Y, HUANG W, LU K F, et al. Modeling and finite-time control for the hypersonic morphing flight vehicle. Journal of Beijing University of Aeronautics and Astronautics, 2022, 48(10): 1979–1993. (in Chinese)